

Geometrical Sensor Selection in Large-Scale High-Density Sensor Networks

Gholamreza Alirezaei and Johannes Schmitz
 Institute for Theoretical Information Technology
 RWTH Aachen University, D-52056 Aachen, Germany
 Email: {alirezaei, schmitz}@ti.rwth-aachen.de

Abstract—In this paper, we consider large-scale high-density sensor networks consisting of small battery-powered sensor nodes. As these sensors are heavily limited in terms of energy consumption and thus the lifetime of the entire network is restricted, it is reasonable to introduce a sensor power as well as a total network power constraint. Both power constraints can simultaneously hold by means of smart power allocation methods. For a large number of sensor nodes the complexity of the utilized selection algorithm can become intolerably high. In order to simplify the power allocation procedure as well as a consecutive selection of most reliable sensor nodes, we propose an analytic-geometric pre-selection of 3-dimensional subspaces, in which more reliable sensor nodes are located. Our investigation is based on the distance between uniformly distributed sensor nodes, the target object and the fusion center as well as a free space signal propagation model. We present analytical solutions for the selection procedure and derive simplified equations in order to directly determine the region of active sensor nodes in closed-form.

I. INTRODUCTION

A certain type of conceivable future sensor networks consists of extremely large numbers of small sensor nodes [1]. This might go as far as the dispersal of thousands of micro-scale sensor nodes (SNs) forming a smart-dust [2]. Application examples range from underwater networks [3] to habitat monitoring [4]. Today, recent developments and technologies in the space industry enable designing miniaturized satellites ranging down to femtosatellites [5]. While a smart-dust cloud of devices in the orbit is theoretically examined in [6], the paper [7] describes a practical demonstration in space. A cloud of such mini-satellites may be modeled as a sensor network. These large-scale sensor networks regularly rely on battery or solar powered devices, which are highly limited in terms of their power consumption and transmission power. The consideration of a total network power constraint, which might be realized based on an intelligent method for sensor selection in conformance with application requirements, is a well-known approach to improve the lifetime and efficiency of the entire network. The complexity of algorithms for an optimal sensor selection, as presented for example in [8], scales with the number of devices. Other approaches like [9] and [10] explicitly try to maximize the lifetime of a battery powered sensor network. In [11], we have studied and optimized the sensor selection and power allocation for a specific passive sensor network with respect to the sensing application. Moreover, an active radar sensor network is similarly examined and the power allocation is analytically optimized in closed-form in [12].

Instead of searching for selection algorithms, we are aiming for an analytic-geometric solution of the same active radar problem as in [12], where regions containing subsets of most

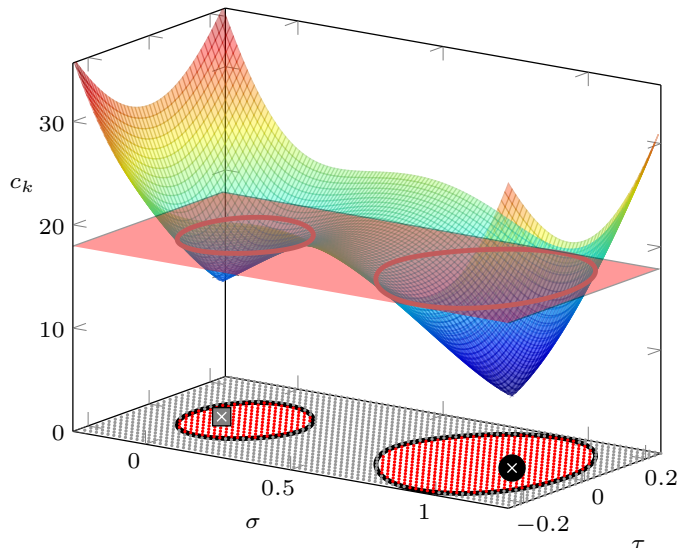


Fig. 1. A visualization of the 2-d reliability-function containing the slice plane and its projection. Active and idle sensor nodes are marked in red and gray, respectively. The fusion center and the target object are marked by a square and a circle, respectively.

reliable, and therefore active, SNs are determined. In general, as depicted in Figure 1, only a single region, not necessary a connected space, exists such that all containing SNs are active and correspond with the optimum power allocation. Figure 1 shows a cut through the reliability-function yielding the optimum selection area of SNs in a 2-dimensional case, where all SNs, the fusion center and the target object are placed on a single plane. In the present paper, assuming a uniform distribution of SNs and a simple channel model without multipath and fading effects, we are able to determine 3-dimensional subspaces for identifying the most reliable SNs. Although the mathematical integration for determining the number of active SNs within the corresponding geometrical subspace is challenging, we analytically derive novel relationships in closed-form between the number of active SNs, their reliability and geometrical positions. Since these results are cumbersome in practice, we propose accurate and integrable approximations of the original subspace providing again closed-form solutions. Our insights might be used for replacing the selection procedure or for pre-selection of most reliable SNs to limit the complexity of subsequent algorithms.

Conventions and mathematical notations:

In order to distinguish the current operating mode of each SN in what follows, we say a SN is *inactive* or *idle* if the allocated power is zero. We say a SN is *active* if the allocated

power is positive. An overview of all notations that we will use hereinafter and are needed for the description of each observation process is depicted in Table I.

Throughout this paper we denote the sets of natural, integer, real, and complex numbers by \mathbb{N} , \mathbb{Z} , \mathbb{R} , and \mathbb{C} , respectively. The imaginary unit is denoted by j . Note that the set of natural numbers does not include the element zero. Moreover, \mathbb{R}_+ denotes the set of non-negative real numbers. Furthermore, we use the subset $\mathbb{F}_N \subseteq \mathbb{N}$ which is defined as $\mathbb{F}_N := \{1, \dots, N\}$ for any given natural number N . We denote the absolute value of a real or complex-valued number z by $|z|$ while the expected value of a random variable v is denoted by $\mathcal{E}[v]$. The logical conjunction is marked as \wedge .

II. OVERVIEW AND TECHNICAL SYSTEM DESCRIPTION

In the following, we shortly describe the underlying system model that is depicted in Figure 2. A detailed description and specification of the whole system can be found in [12]. Hereafter, the continuous-time system is modeled by its discrete-time baseband equivalent, where the sampling rate of the corresponding signals is equal to the target observation rate, for the sake of simplicity. Moreover, we disregard time delays within all transmissions and assume synchronized data communication.

At any instance of time, a network of $K \in \mathbb{N}$ independent and spatially distributed SNs receives random observations. If a target object is present, then the received power at the SN S_k is a part of its own emitted power, which is back-reflected from the jointly observed target object and is weighted by its reflection coefficient $r_i \in \mathbb{C}$, $i \in \mathbb{F}_I$, with $r_{\text{rms}}^2 := \mathcal{E}[|r_i|^2]$ and $0 < r_{\text{rms}} < \infty$. The object may be of I different types. It should be noted that sheer detection may be treated as the special case of $I = 2$ which corresponds to the decision ‘*some object is present*’ versus ‘*there is no object*’. We assume that all different object types and their corresponding reflection coefficients are known by the network and the actual target object is assumed to behave static during several consecutive observation steps. Each received signal is in addition weighted by the corresponding channel coefficient $g_k \in \mathbb{C}$ and is disturbed by additive white Gaussian noise (AWGN) $m_k \in \mathbb{C}$ with $M_0 := \mathcal{E}[|m_k|^2] < \infty$. We assume in this paper that all sensing channels are constants. Thus, the expected value and the quadratic mean of each coefficient are described by $\mathcal{E}[g_k] = g_k$ and $\mathcal{E}[|g_k|^2] = |g_k|^2$, respectively. The sensing channel is obviously wireless.

We model each SN by an amplify-and-forward unit with extended capabilities, where both sensing and communication signals are transmitted simultaneously. The sensing signal w_k , without loss of generality, is assumed to be non-negative, real-valued and deterministic. The expected value of its instantaneous power is then described by

$$W_k := \mathcal{E}[|w_k|^2] = |w_k|^2, \quad k \in \mathbb{F}_K. \quad (1)$$

Note that the specific value of w_k is adjustable and will be determined later by the power allocation procedure.

The ratio of the communication signal to the received sensing signal is described by the non-negative real-valued amplification factor u_k which is assumed to be constant over the whole bandwidth and power-range. Thus, the communication

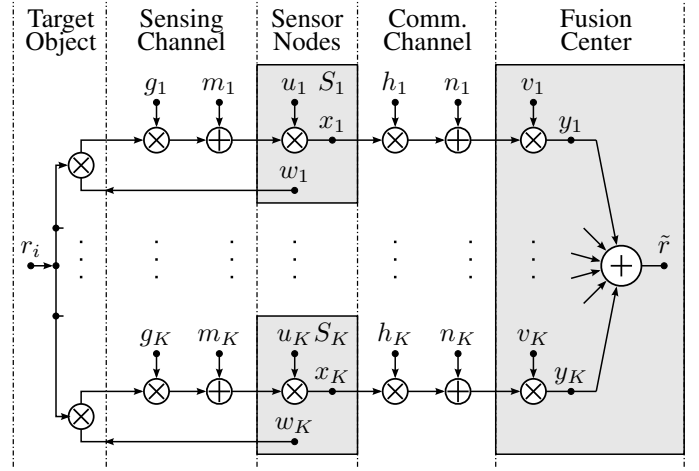


Fig. 2. System model of the distributed active sensor network.

signal and the expected value of its instantaneous power are described by

$$x_k := (r_i g_k w_k + m_k) u_k, \quad k \in \mathbb{F}_K \quad (2)$$

and

$$X_k := \mathcal{E}[|x_k|^2] = (r_{\text{rms}}^2 |g_k|^2 W_k + M_0) u_k^2, \quad k \in \mathbb{F}_K, \quad (3)$$

respectively. The amplification factor is an adjustable parameter and will be determined later by the power allocation procedure, as well. Note that the instantaneous power fluctuates from observation to observation depending on the present target object.

If the received signal is negligible in comparison to the output signal and if the nodes have smart power components with low-power dissipation loss, then the average power consumption of each node is approximately equal to its average output power $W_k + X_k$. The addition of both transmission powers is justified because the corresponding signals are assumed to be separated by distinct waveforms. We also assume that the output power-range of each SN is limited by P_{max} and that the average power consumption of all SNs together is limited by the sum-power constraint P_{tot} . Hence, the constraints

$$W_k + X_k \leq P_{\text{max}}, \quad k \in \mathbb{F}_K \quad (4)$$

and

$$\sum_{k \in \mathbb{F}_K} \underbrace{W_k}_{\text{Radar task}} + \underbrace{X_k}_{\text{Data communication}} \leq P_{\text{tot}} \quad (5)$$

Average transmission power of one sensor for a single observation

arise consequently.

After amplification of the received sensing signal, all local observations are then transmitted to a fusion center, which is placed in a remote location. The communication to the fusion center is performed by using distinct waveforms for each SN so as to distinguish the communication of different SNs. Each waveform has to be suitably chosen in order to suppress inter-user (inter-node) interference at the fusion center. Hence, all K received signals at the fusion center are pairwise uncorrelated and are assumed to be conditionally independent. Each received signal at the fusion center is also weighted by the corresponding channel coefficient $h_k \in \mathbb{C}$

and is disturbed by additive white Gaussian noise $n_k \in \mathbb{C}$ with $N_0 := \mathcal{E}[|n_k|^2] < \infty$, as well. We also assume in this paper that all communication channels are constants. Thus, the expected value and the quadratic mean of each coefficient are described by $\mathcal{E}[h_k] = h_k$ and $\mathcal{E}[|h_k|^2] = |h_k|^2$, respectively. The data communication between each SN and the fusion center can either be wireless or wired.

The noisy received signals at the fusion center are weighted by $v_k \in \mathbb{C}$ and combined together in order to obtain a single reliable observation \tilde{r} of the reflection coefficient r_i of the actual target object. In this way, we obtain

$$y_k := (x_k h_k + n_k) v_k, \quad k \in \mathbb{F}_K, \quad (6)$$

and hence,

$$\tilde{r} := \sum_{k=1}^K y_k = r_i \sum_{k=1}^K w_k g_k u_k h_k v_k + \sum_{k=1}^K (m_k u_k h_k + n_k) v_k. \quad (7)$$

Note that each weight can be written as $v_k = |v_k| \exp(j\vartheta_k)$, $k \in \mathbb{F}_K$, where ϑ_k is a real-valued number which represents the phase of the corresponding weight.

Note that the fusion center can separate all input streams because the data communication is either wired or performed by distinct waveforms for each SN. Consequently, if the communication channel is wireless then a matched-filter bank is essential at the input of the fusion center to separate data streams of different SNs. In addition, we do not consider inter-user (inter-node) interferences at the fusion center because of the distinct waveform choices.

In order to obtain a single reliable observation at the fusion center, the value \tilde{r} should be a good estimate for the present reflection coefficient r_i . Thus, we optimize the sensing power W_k , the amplification factors u_k , and the weights v_k in order to minimize the average absolute deviation between \tilde{r} and the true reflection coefficient r_i . This optimization and its solution are elaborately explained in the next section. After determining the optimal values for W_k , u_k and v_k , the fusion center observes a disturbed version of the true reflection coefficient r_i at the input of its decision unit. Hence, by using the present system model, we are able to separate the power allocation problem from the classification problem and optimize both independently.

III. SENSOR SELECTION

In this section, we introduce the power optimization problem and present its optimal solution from [12] in a concise form. Two different power constraints are simultaneously considered, a sum-power constraint $P_{\text{tot}} \in \mathbb{R}_+$ for the cumulative sum of the expected power consumption of each SN as well as a limitation of the average transmission power of each SN by $P_{\text{max}} \in \mathbb{R}_+$. Afterwards, we investigate the problem of sensor selection in any 3-dimensional space which is important for a fast power allocation in large-scale high-density sensor networks.

A. Optimization problem

As mentioned in the last section, the value \tilde{r} should be a good estimate for the actual reflection coefficient r_i of

TABLE I. NOTATION OF SYMBOLS THAT ARE NEEDED FOR THE DESCRIPTION OF EACH OBSERVATION PROCESS.

Notation	Description
K, \bar{K}	the number of all nodes and all active nodes;
\mathbb{F}_K	the index-set of K nodes;
I	number of different reflection coefficients;
r_i	reflection coefficient of i^{th} target object;
r_{rms}	root mean squared absolute value of reflection coefficients;
\tilde{r}	estimate of the actual reflection coefficient r_i ;
g_k, h_k	complex-valued channel coefficients;
d_{g_k}, d_{h_k}	distances from k^{th} sensor node to target object and to fusion center;
m_k, n_k	complex-valued zero-mean AWGN;
M_0, N_0	variances of m_k and n_k ;
u_k, v_k	non-negative amplification factors and complex-valued weights;
ϑ_k, ϕ_k	phase of v_k and phase of the product $g_k h_k$;
w_k, x_k	sensing and communication signal of k^{th} sensor node;
W_k, X_k	sensing and communication power of k^{th} sensor node;
y_k	input signals of the combiner;
$c_k(P)$	reliability of k^{th} sensor node working with transmission power P ;
$(\sigma_k, \tau_k, \omega_k)$	position of k^{th} sensor node in Cartesian coordinates;
$P_{\text{max}}, P_{\text{tot}}$	output power-range limitation and sum-power constraint;
λ	signal wavelength;
ρ	density of sensor nodes per volume unit.

the present target object. In particular, we aim at finding estimators \tilde{r} of minimum mean squared error in the class of unbiased estimators for each $i \in \mathbb{F}_I$. The estimate \tilde{r} is unbiased simultaneously for each i if $\mathcal{E}[\tilde{r} - r_i] = 0$, i.e., from equation (7) and (1) we obtain the identity

$$\sum_{k=1}^K \sqrt{W_k} g_k u_k h_k |v_k| \exp(j\vartheta_k) = 1. \quad (8)$$

This identity is our first constraint in what follows. The objective is to minimize the mean squared error $\mathcal{E}[|\tilde{r} - r_i|^2]$. By using equation (7) and the identity (8) we may write the objective function as

$$V := \mathcal{E}[|\tilde{r} - r_i|^2] = \sum_{k=1}^K |v_k|^2 (u_k^2 |h_k|^2 M_0 + N_0). \quad (9)$$

As mentioned in the last section, each SN has an output power-range limitation and the expected overall power consumption is also limited. Hence, the objective function is also subject to (4) and (5), which are our second and last constraints, respectively.

In summary, the optimization problem is to minimize the mean squared error in (9) with respect to u_k , v_k , and W_k , subject to constraints (4), (5) and (8).

B. Optimal allocation of transmission power

In the current subsection, we consider the optimization problem from Subsection III-A and highlight corresponding main results from [12] that are necessary for the present paper.

Without loss of generality, we set the useful range of P_{max} and P_{tot} equal to $0 < P_{\text{max}} \leq P_{\text{tot}} \leq K P_{\text{max}}$ and assume the quantization of the sum-power constraint by $\frac{P_{\text{tot}}}{P_{\text{max}}} \in \mathbb{N}$ for reasons of simplicity. By solving the above power optimization problem, a specific quantity for the reliability of each SN is given as

$$c_k(P) := \sqrt{\alpha_k \beta_k} + \sqrt{(\alpha_k + P)(\beta_k + P)}, \quad k \in \mathbb{F}_K, P \in \mathbb{R}_+, \quad (10)$$

where for the sake of simplicity, both notations

$$\alpha_k := \frac{M_0}{r_{\text{rms}}^2 |g_k|^2} \quad \text{and} \quad \beta_k := \frac{N_0}{|h_k|^2}, \quad \alpha_k, \beta_k \in \mathbb{R}_+, \quad (11)$$

are used. If all SNs are such re-indexed that the inequality chain

$$c_k(P_{\max}) \leq c_{k+1}(P_{\max}), \quad k \in \mathbb{F}_{K-1}, \quad (12)$$

holds, then the reliability of the best and the worst SN is described by c_1 and c_K , respectively. Since the reliability of the first \tilde{K} SNs, with $\tilde{K} \in \mathbb{N}$ and $1 \leq \tilde{K} \leq K$, is better than that of the remaining ones, only these \tilde{K} SNs are active and participate in sensing and data communication. Each of \tilde{K} SNs receives P_{\max} for the sum of its sensing and communication powers.

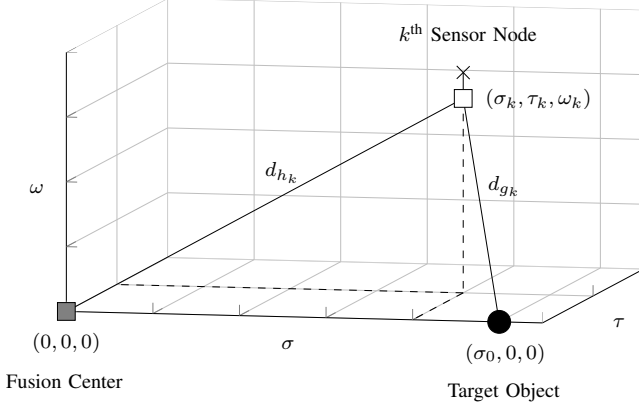


Fig. 3. The placement of fusion center, target object and all sensor nodes in Cartesian coordinates.

C. Identifying the best sensor nodes

The main problem of sensor selection is to sort all SNs such that the inequality chain in (12) holds. Since each quantity $c_k(P_{\max})$ is dependent on its $|g_k|$ and $|h_k|$, the geometric position of fusion center, target object and k^{th} -SN pre-describe the expected value of $c_k(P_{\max})$. Thus, for selecting the most reliable SNs, an investigation of the interaction of all positions is essential. In the following, we consider a scenario described by Figure 3, where the fusion center is located at the origin of the Cartesian coordinates, the target object at the position $(\sigma_0, 0, 0)$, $\sigma_0 \in \mathbb{R}_+$, and the k^{th} -SN at the position $(\sigma_k, \tau_k, \omega_k) \in \mathbb{R}^3$. If we only consider the free-space path loss without fading, then both channel coefficients of the k^{th} -SN are described by

$$|g_k| = \frac{\lambda}{4\pi^2 d_{g_k}} \quad \text{and} \quad |h_k| = \frac{\lambda}{4\pi d_{h_k}}, \quad k \in \mathbb{F}_K, \quad (13)$$

where the distance between the SN to the fusion center is described by $d_{h_k} \in \mathbb{R}_+$ while the distance from the SN to the target object and back to the same SN is described by $2d_{g_k} \in \mathbb{R}_+$. The value λ is the signal wavelength. Both Euclidean distances d_{g_k} and d_{h_k} are described by

$$d_{g_k} := \sqrt{(\sigma_k - \sigma_0)^2 + \tau_k^2 + \omega_k^2}, \quad k \in \mathbb{F}_K, \quad (14)$$

and

$$d_{h_k} := \sqrt{\sigma_k^2 + \tau_k^2 + \omega_k^2}, \quad k \in \mathbb{F}_K. \quad (15)$$

By incorporating all above equations into (10) and (11), we obtain

$$c_k(P) = \sqrt{a^2 [(\sigma_k - \sigma_0)^2 + \tau_k^2 + \omega_k^2]} \sqrt{b^2 [\sigma_k^2 + \tau_k^2 + \omega_k^2]} + \sqrt{P + a^2 [(\sigma_k - \sigma_0)^2 + \tau_k^2 + \omega_k^2]} \sqrt{P + b^2 [\sigma_k^2 + \tau_k^2 + \omega_k^2]}, \quad (16)$$

where both parameters a and b are independent from index k and are given as

$$a^2 := \frac{M_0 4^3 \pi^2}{\lambda^2 r_{\text{rms}}^2} > 0 \quad \text{and} \quad b^2 := \frac{N_0 4^2 \pi^2}{\lambda^2} > 0. \quad (17)$$

For a given c and P_{\max} , with $c_1(P_{\max}) \leq c \leq c_K(P_{\max})$, the associated subspace $\mathbb{S}_0(c)$, in which the most reliable SNs with $c_k(P_{\max}) \leq c$ for some k are included, is described with the aid of (16) by

$$\mathbb{S}_0(c) := \{(\sigma, \tau, \omega) \in \mathbb{R}^3 \mid \sqrt{a^2 [(\sigma - \sigma_0)^2 + \tau^2 + \omega^2]} \cdot \sqrt{b^2 [\sigma^2 + \tau^2 + \omega^2]} + \sqrt{P_{\max} + b^2 [\sigma^2 + \tau^2 + \omega^2]} \cdot \sqrt{P_{\max} + a^2 [(\sigma - \sigma_0)^2 + \tau^2 + \omega^2]} \leq c\}. \quad (18)$$

The surface of the subspace (18) describes a 2-dimensional submanifold, a 3-dimensional subspace of \mathbb{R}^3 , which in turn is described by a multivariate polynomial with a degree equal to four in three variables and five parameters. Thus, it is analytically challenging to calculate its volume in closed-form, since for this calculation the evaluation of all polynomial roots is needed to obtain the integration boundaries. Nevertheless, in the following, we set out to obtain a relationship between the number \tilde{K} of active SNs and corresponding values of the reliability-function $c_k(P_{\max})$ by calculating the volume of (18).

At first, we reduce the number of parameters by the substitutions $P_a := P_{\max}/a^2$, $P_b := P_{\max}/b^2$ and $c_{ab} := c/(a \cdot b)$. Second, we reduce the number of variables for integration by transforming the coordinate system with the aid of $\xi^2 := \tau^2 + \omega^2$, since \mathbb{S}_0 is symmetric with respect to rotations in the τ - ω -plane. Hence, we obtain two equivalent forms

$$\begin{aligned} \mathbb{S}_0(c_{ab}) &= \{(\sigma, \xi, \varphi) \in \mathbb{R} \times \mathbb{R}_+ \times [0, 2\pi] \mid \sqrt{(\sigma - \sigma_0)^2 + \xi^2} \\ &\cdot \sqrt{\sigma^2 + \xi^2} + \sqrt{P_b + \sigma^2 + \xi^2} \sqrt{P_a + (\sigma - \sigma_0)^2 + \xi^2} \leq c_{ab}\} \\ &= \{(\sigma, \xi) \in \mathbb{R} \times \mathbb{R}_+ \mid \sqrt{(\sigma - \sigma_0)^2 + \xi^2} \sqrt{\sigma^2 + \xi^2} \\ &+ \sqrt{P_b + \sigma^2 + \xi^2} \sqrt{P_a + (\sigma - \sigma_0)^2 + \xi^2} \leq c_{ab}\} \times [0, 2\pi] \\ &=: \tilde{\mathbb{S}}_0(c_{ab}) \times [0, 2\pi]. \quad (19) \end{aligned}$$

In order to calculate the corresponding number \tilde{K}_0 of SNs, which are members of the subspace $\mathbb{S}_0(c_{ab})$, an integration over the sensor distribution in this subspace is needed. If we assume that all SNs are uniformly distributed, with a density of ρ SNs per volume-unit, then we are analytically able to calculate the corresponding integrals

$$\tilde{K}_0(c_{ab}) := \int_{\mathbb{S}_0(c_{ab})} \rho \, d\sigma \, d\tau \, d\omega = 2\pi \int_{\tilde{\mathbb{S}}_0(c_{ab})} \rho \, \xi \, d\sigma \, d\xi \quad (20)$$

in closed form. However, for the integration all proper boundaries are needed. These boundaries are equivalent with some real roots of the equation

$$\begin{aligned} &\sqrt{(\sigma - \sigma_0)^2 + \xi^2} \sqrt{\sigma^2 + \xi^2} \\ &+ \sqrt{P_b + \sigma^2 + \xi^2} \sqrt{P_a + (\sigma - \sigma_0)^2 + \xi^2} - c_{ab} = 0. \quad (21) \end{aligned}$$

By some algebra, we infer four real roots for ξ while only one of them can be satisfied by the range of σ and is in addition

always positive. The corresponding root is given by

$$\begin{aligned} \xi_0^2(\sigma) := & \left[(P_a + P_b)[2c_{ab}^2 - 2P_aP_b - \sigma_0(P_a - P_b)(2\sigma - \sigma_0)] \right. \\ & + (2\sigma^2 + \sigma_0^2 - 2\sigma\sigma_0)[4c_{ab}^2 - (P_a + P_b)^2] \\ & - 4c_{ab}\sqrt{c_{ab}^2 - (P_a - 2\sigma\sigma_0 + \sigma_0^2)(P_b + 2\sigma\sigma_0 - \sigma_0^2)} \\ & \left. \cdot \sqrt{c_{ab}^2 - P_aP_b} \right] / [2(P_a + P_b)^2 - 8c_{ab}^2]. \end{aligned} \quad (22)$$

Furthermore, we infer four roots for σ which define possible integration boundaries over σ and in turn yield real positive values for $\xi_0^2(\sigma)$. The first two roots of σ are always real while the domain of the other two is real or complex depending on a certain choices of parameters. These roots are given as

$$\sigma_1 := \frac{2\sigma_0(P_b + c_{ab}) - \sqrt{c_{ab}^2 - P_aP_b}\sqrt{P_a + P_b + 2c_{ab} + \sigma_0^2}}{2(P_a + P_b + 2c_{ab})}, \quad (23a)$$

$$\sigma_2 := \frac{2\sigma_0(P_b + c_{ab}) + \sqrt{c_{ab}^2 - P_aP_b}\sqrt{P_a + P_b + 2c_{ab} + \sigma_0^2}}{2(P_a + P_b + 2c_{ab})}, \quad (23b)$$

$$\sigma_3 := \frac{2\sigma_0(P_b - c_{ab}) - \sqrt{c_{ab}^2 - P_aP_b}\sqrt{P_a + P_b - 2c_{ab} + \sigma_0^2}}{2(P_a + P_b - 2c_{ab})}, \quad (23c)$$

and

$$\sigma_4 := \frac{2\sigma_0(P_b - c_{ab}) + \sqrt{c_{ab}^2 - P_aP_b}\sqrt{P_a + P_b - 2c_{ab} + \sigma_0^2}}{2(P_a + P_b - 2c_{ab})}. \quad (23d)$$

Since the subspace $\mathbb{S}_0(c_{ab})$ is for some certain choices of parameters a connected space and for other choices a disconnected space, different cases for the evaluation of the integral (20) are to distinguish. In summary, we obtain the following five cases.

- 1) If $c_{ab} \leq \min\{\sqrt{(P_b + \sigma_0^2)P_a}, \sqrt{(P_a + \sigma_0^2)P_b}\}$, the value of c_{ab} is too small to obtain any positive volume:

$$\Rightarrow \tilde{K}_0(c_{ab}) = 0 \quad (24a)$$

- 2) If $\min\{\sqrt{(P_b + \sigma_0^2)P_a}, \sqrt{(P_a + \sigma_0^2)P_b}\} < c_{ab} \wedge P_a > P_b \wedge c_{ab} \leq \max\{\sqrt{(P_b + \sigma_0^2)P_a}, \sqrt{(P_a + \sigma_0^2)P_b}\}$, the subspace \mathbb{S}_0 is a disconnected space and separated in two regions, where only one of both regions has a positive real volume:

$$\Rightarrow \tilde{K}_0(c_{ab}) = \pi\rho \int_{\sigma_1}^{\sigma_4} \xi_0^2(\sigma) d\sigma \quad (24b)$$

- 3) If $\min\{\sqrt{(P_b + \sigma_0^2)P_a}, \sqrt{(P_a + \sigma_0^2)P_b}\} < c_{ab} \wedge P_a < P_b \wedge c_{ab} \leq \max\{\sqrt{(P_b + \sigma_0^2)P_a}, \sqrt{(P_a + \sigma_0^2)P_b}\}$, the structure of the subspace \mathbb{S}_0 is analogous to the previous case:

$$\Rightarrow \tilde{K}_0(c_{ab}) = \pi\rho \int_{\sigma_3}^{\sigma_2} \xi_0^2(\sigma) d\sigma \quad (24c)$$

- 4) If $\max\{\sqrt{(P_b + \sigma_0^2)P_a}, \sqrt{(P_a + \sigma_0^2)P_b}\} < c_{ab} \leq \frac{P_a + P_b + \sigma_0^2}{2} \wedge \sigma_0^2 > |P_b - P_a|$, the disconnected subspace \mathbb{S}_0 consists of two regions and has two positive real volumes:

$$\Rightarrow \tilde{K}_0(c_{ab}) = \pi\rho \int_{\sigma_1}^{\sigma_4} \xi_0^2(\sigma) d\sigma + \pi\rho \int_{\sigma_3}^{\sigma_2} \xi_0^2(\sigma) d\sigma \quad (24d)$$

- 5) If otherwise, then the subspace \mathbb{S}_0 is a connected space with a single positive volume:

$$\Rightarrow \tilde{K}_0(c_{ab}) = \pi\rho \int_{\sigma_1}^{\sigma_2} \xi_0^2(\sigma) d\sigma. \quad (24e)$$

Note that for the above cases the unbounded integral $\int \xi_0^2(\sigma) d\sigma$ is given in closed-form with the aid of [13, p. 95, eq. 2.262.1] and [13, p. 94, eq. 2.261]. Unfortunately, this solution is too long such that we omit the presentation of this integration result in the present paper, for the sake of compactness.

All equations in (24) analytically determine the number \tilde{K}_0 of active SNs as a function of any maximum reliability value c_{ab} in closed-form. These are the main contributions of the present paper.

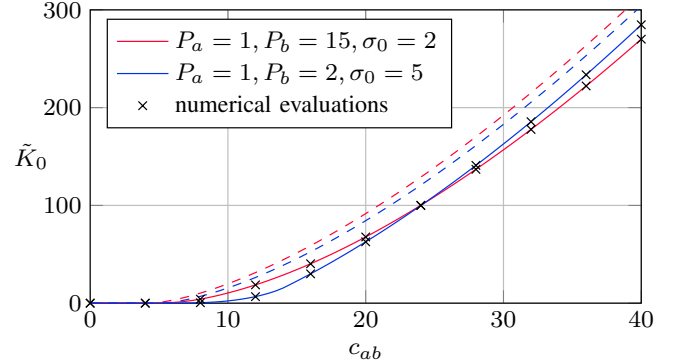


Fig. 4. Number \tilde{K}_0 of active sensor nodes, which are included in the subspace $\mathbb{S}_0(c_{ab})$, as a function of the maximum reliability c_{ab} for $\rho = 1$. Two different sets of parameters are chosen to visualize all five cases described analytically by equations in (24). Markers show numerical evaluations of (20) for comparison. Equation (32) is also visualized by two dashed curves for the same two sets of parameters.

D. Approximations for the number of active sensor nodes

Although the results in (24) are in closed-form, they are cumbersome for practical applications. In practice, there is a need for a fast evaluation of the number \tilde{K}_0 of active SNs for a given maximum reliability value especially in large-scale high-density sensor networks. Since in a high-density sensor networks the exact number of active SNs plays a minor part while an accurate approximation of this number is adequate in most cases, we set out to approximate the subspace in (18) by simpler upper and lower bounds of (16) in the following in order to obtain approximations for the number of active SNs.

By applying the Cauchy-Schwarz inequality [14], we infer for the righthand side of (16) the upper bound

$$P + a^2 [(\sigma_k - \sigma_0)^2 + \tau_k^2 + \omega_k^2] + b^2 [\sigma_k^2 + \tau_k^2 + \omega_k^2] \quad (25)$$

and the lower bound

$$P + \frac{2ab}{3} [|\sigma_k - \sigma_0|(|\sigma_k| + |\tau_k| + |\omega_k|) + (|\tau_k| + |\omega_k|)^2 + |\sigma_k|(|\tau_k| + |\omega_k|)]. \quad (26)$$

From these bounds we obtain the subspaces

$$\mathbb{S}_1(c) := \{(\sigma, \tau, \omega) \in \mathbb{R}^3 \mid a^2 [(\sigma - \sigma_0)^2 + \tau^2 + \omega^2] + P_{\max} + b^2 [\sigma^2 + \tau^2 + \omega^2] \leq c\} \quad (27)$$

and

$$\mathbb{S}_2(c) := \{(\sigma, \tau, \omega) \in \mathbb{R}^3 \mid [|\sigma - \sigma_0|(|\sigma| + |\tau| + |\omega|) + (|\tau| + |\omega|)^2 + |\sigma|(|\tau| + |\omega|)] \frac{2ab}{3} + P_{\max} \leq c\}. \quad (28)$$

Note that by the upper bound a smaller subspace $\mathbb{S}_1(c)$, and by the lower bound a larger subspace $\mathbb{S}_2(c)$ is described for the

same value of c . In summary we have $\mathbb{S}_1(c) \subseteq \mathbb{S}_0(c) \subseteq \mathbb{S}_2(c)$, thus far. In order to calculate the corresponding number of SNs, which are members of the subspace $\mathbb{S}_2(c)$ or even $\mathbb{S}_1(c)$, an integration over the sensor distribution in these subspaces is again needed. If we assume uniformly distributed SNs, then we are analytically able to calculate the corresponding integrals

$$\tilde{K}_1(c) := \int_{\mathbb{S}_1(c)} \rho \, d\sigma \, d\tau \, d\omega \quad \text{and} \quad \tilde{K}_2(c) := \int_{\mathbb{S}_2(c)} \rho \, d\sigma \, d\tau \, d\omega \quad (29)$$

in closed form. The number of SNs included in the subspace $\mathbb{S}_1(c)$ is then equal to

$$\tilde{K}_1(c) = \frac{4\rho\pi}{3} \left(\frac{\sqrt{(a^2 + b^2)(c - P_{\max}) - a^2 b^2 \sigma_0^2}}{a^2 + b^2} \right)^3, \quad (30)$$

for all c , P_{\max} , a and b for which the discriminant is nonnegative. The correct expression for the number of SNs included in the subspace $\mathbb{S}_2(c)$ is complicated such that we use a simpler upper bound given by the cases

$$\tilde{K}_2(c) = \rho \cdot \begin{cases} \left(\frac{6(c - P_{\max})}{ab\sigma_0} \right)^3 \left(\frac{1}{24} - \frac{6(c - P_{\max})}{91ab\sigma_0^2} \right), \\ \left(\frac{\sigma_0^2}{6^{2/3}} + \frac{c - P_{\max}}{ab6^{-1/3}} \right)^{3/2} + \frac{7\sigma_0^3}{118} - \sqrt{\frac{3\sigma_0^4(c - P_{\max})}{2ab}}, \end{cases} \quad (31)$$

where the first and second case for $\frac{\sigma_0^2}{6} \geq \frac{c - P_{\max}}{ab} > 0$ and $\frac{c - P_{\max}}{ab} > \frac{\sigma_0^2}{6}$ hold, respectively.

In general, it holds that $0 \leq \tilde{K}_1(c) \leq \tilde{K}_0(c) \leq \tilde{K}_2(c)$. The concrete difference of these numbers is dependent on all included parameters and is discussed for some special cases in the next section.

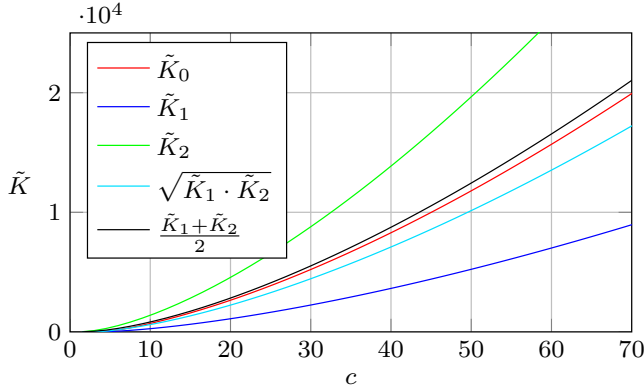


Fig. 5. Number of sensor nodes included in the subspaces. The parameters are: $\rho = 1$, $a = 0.6$, $b = 0.2$, $P_{\max} = 10^{-5}$ and $\sigma_0 = 10$.

E. Extensions and improvements

It is to mention that proposed solutions are improvable in various ways. We highlight two types of improvements here:

1: Since the value of \tilde{K}_0 is analytically determined by equations (24), it is possible to obtain more accurate approximations for \tilde{K}_0 by bounding the equations (24) instead of bounding the subspace \mathbb{S}_0 . For instance, the approximation of (24e) by

$$\tilde{K}_0(c_{ab}) \approx \frac{\pi\rho\sqrt{2} \left(c_{ab} - \min \left\{ \sqrt{(P_b + \sigma_0^2)P_a}, \sqrt{(P_a + \sigma_0^2)P_b} \right\} \right)^{\frac{3}{2}}}{3}, \quad (32)$$

for all $c_{ab} \gg \frac{P_a + P_b + \sigma_0^2}{2}$, is on the one hand very simple and on the other hand quite accurate.

2: In general, better lower and upper bounds for the subspace $\mathbb{S}_0(c)$ exist which however are not integrable in closed-form. Some other examples of bounds, which are integrable or their integral is approximable in closed-form, are for instance described by

$$\left\{ (\sigma, \tau, \omega) \in \mathbb{R}^3 \mid \sqrt{P_{\max} + 2a^2[(\sigma - \sigma_0)^2 + \tau^2 + \omega^2]} \cdot \sqrt{P_{\max} + 2b^2[\sigma^2 + \tau^2 + \omega^2]} \leq c \right\}, \quad (33)$$

which is a better bound than $\mathbb{S}_1(c)$, or by an optimized combination of the expressions

$$|\sigma - \sigma_0||\sigma|, \tau^2 + \omega^2, |\tau\omega|, |\sigma - \sigma_0|(|\tau| + |\omega|), |\sigma|(|\tau| + |\omega|), P_{\max} \quad \text{and} \quad \sqrt{P_{\max}}(a[|\sigma - \sigma_0| + |\tau| + |\omega|] + b[|\sigma| + |\tau| + |\omega|]) \quad (34)$$

which would yield a better bound than $\mathbb{S}_2(c)$.

The investigation of these and further extensions are devoted to future works.

IV. VISUALIZATION AND NUMERICAL RESULTS

In Figure 4, the relationship between the number \tilde{K}_0 of active SNs and the maximum reliability c_{ab} is shown for two different sets of parameters. All markers represent numerical evaluations while all continuous curves represent analytical results. Furthermore, the approximation in (32) is depicted which converges very fast for large values of c_{ab} .

In order to develop an imagination of the different subspaces, the surfaces of all three subspaces are exemplary depicted in Figure 6 for the same values of parameters. As we can see, the relation $\mathbb{S}_1(c) \subseteq \mathbb{S}_0(c) \subseteq \mathbb{S}_2(c)$ holds. Moreover, the subspace $\mathbb{S}_0(c)$ is an accurate fit for $\mathbb{S}_1(c)$ while the subspace $\mathbb{S}_2(c)$ is an accurate fit for $\mathbb{S}_0(c)$. However, the volume of the subspace $\mathbb{S}_1(c)$ is approximately one half of the volume of $\mathbb{S}_0(c)$ and in turn the volume of the subspace $\mathbb{S}_0(c)$ is approximately one half of the volume of $\mathbb{S}_2(c)$. This shows that the calculation of the number of active SNs by these subspaces is not accurate at all, as we will see in the following. Nevertheless, with these subspaces, we are primarily able to limit the geometric region in which the most reliable SNs are included.

In Figure 7 the ω -ordinate is fixed to $\omega = 0$ in order to show the effect of the parameter c in conjunction with the slice plane of the corresponding subspaces. Because of a certain choice of the parameters a , b , P_{\max} and σ_0 , it is obvious that the regions become asymmetric and hence for small values of c each single subspace is divided into two parts. This behavior is very clearly shown in Figure 1, as well.

In Figure 5 the number of SNs, which are included in the subspaces $\mathbb{S}_1(c)$, $\mathbb{S}_0(c)$ and $\mathbb{S}_2(c)$, is visualized. Since the approximation of the volumes is not accurate enough, the distances between the curves $\tilde{K}_1(c)$, $\tilde{K}_0(c)$ and $\tilde{K}_2(c)$ are large. Nevertheless, by calculating both geometric and arithmetic means of $\tilde{K}_1(c)$ and $\tilde{K}_2(c)$, both outcomes are comparable with $\tilde{K}_0(c)$. Thus, they can serve as surrogates for accurate approximations of $\tilde{K}_0(c)$.

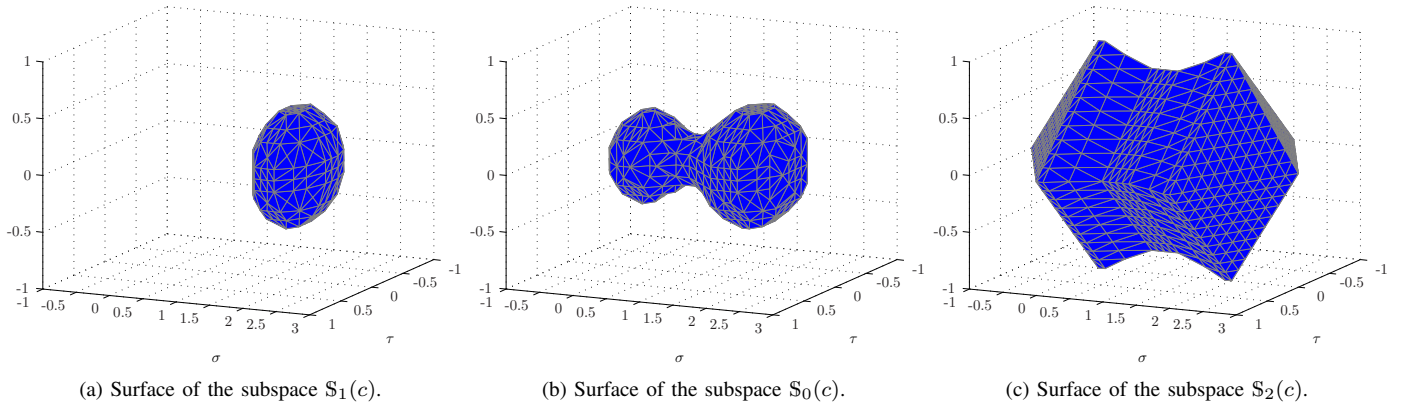


Fig. 6. Visualization of all three subspaces for the choice $a = 0.2$, $b = 0.05$, $c = 0.023$, $P_{\max} = 0.001$ and $\sigma_0 = 2$.

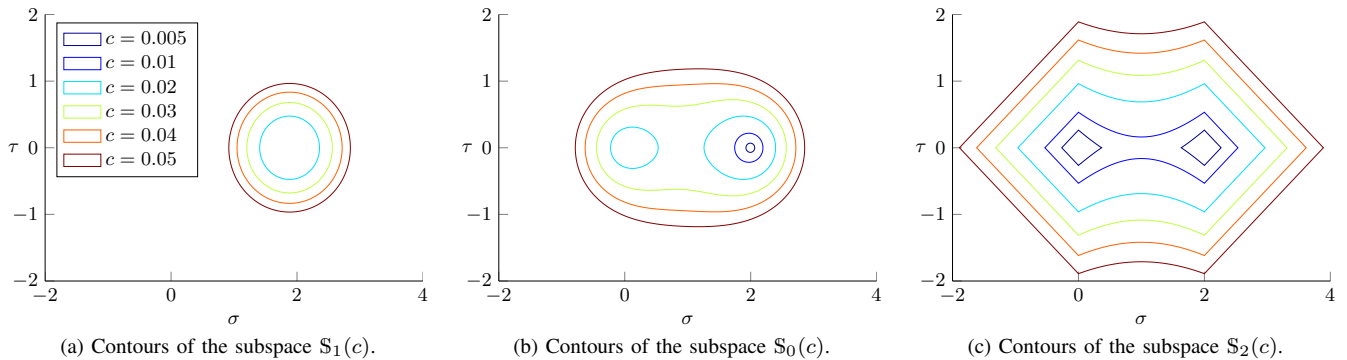


Fig. 7. Visualization of all three subspaces for the choice $a = 0.2$, $b = 0.05$, $P_{\max} = 0.001$ and $\sigma_0 = 2$ while the ω -ordinate is fixed to $\omega = 0$.

V. CONCLUSION

Since a fast sensor selection is a requirement for power control and power allocation in high-density sensor networks, we have introduced a new geometrical approach for this application. Although the structure of the subspace in which all active sensor nodes are located is challenging, we have analytically derived novel relationships in closed-form between the number of active sensor nodes, their reliability-function and geometrical position. Since these results are cumbersome in practical applications, we have proposed two surrogate subspaces with simpler mathematical structures. Both subspaces are again integrable in closed-form such that two further approximations for the relationship between the number of active sensor nodes, their reliability and position are derived. Moreover, with the aid of these subspaces, we are primarily able to limit the geometric region in which the most reliable sensor nodes are included without any numerical evaluation methods.

REFERENCES

- [1] A. Arora, R. Ramnath, E. Ertin, P. Sinha, S. Bapat, V. Naik, V. Kulathumani, H. Zhang, H. Cao, M. Sridharan *et al.*, "Exscal: Elements of an extreme scale wireless sensor network," in *Embedded and Real-Time Computing Systems and Applications, 2005. Proceedings. 11th IEEE International Conference on.* IEEE, 2005, pp. 102–108.
- [2] B. Warneke, M. Last, B. Liebowitz, and K. S. Pister, "Smart dust: Communicating with a cubic-millimeter computer," *Computer*, vol. 34, no. 1, pp. 44–51, 2001.
- [3] J. Heidemann, W. Ye, J. Wills, A. Syed, and Y. Li, "Research challenges and applications for underwater sensor networking," in *Wireless Communications and Networking Conference, 2006. WCNC 2006. IEEE*, vol. 1, April 2006, pp. 228–235.
- [4] R. Szweczyk, A. Mainwaring, J. Polastre, J. Anderson, and D. Culler, "An analysis of a large scale habitat monitoring application," in *Proceedings of the 2nd international conference on Embedded networked sensor systems.* ACM, 2004, pp. 214–226.
- [5] D. J. Barnhart, T. Vladimirova, and M. N. Sweeting, "Very-small-satellite design for distributed space missions," *Journal of Spacecraft and Rockets*, vol. 44, no. 6, pp. 1294–1306, 2007.
- [6] C. Colombo and C. McInnes, "Orbital dynamics of "smart-dust" devices with solar radiation pressure and drag," *Journal of Guidance, Control, and Dynamics*, vol. 34, no. 6, pp. 1613–1631, 2011.
- [7] Z. Manchester, M. Peck, and A. Filo, "Kicksat: A crowd-funded mission to demonstrate the worlds smallest spacecraft," in *Proceedings of the AIAA/USU Conference on Small Satellites*, 2013.
- [8] F. Bian, D. Kempe, and R. Govindan, "Utility based sensor selection," in *Proceedings of the 5th international conference on Information processing in sensor networks.* ACM, 2006, pp. 11–18.
- [9] Q. Dong, "Maximizing system lifetime in wireless sensor networks," in *Information Processing in Sensor Networks, 2005. IPSN 2005. Fourth International Symposium on.* IEEE, 2005, pp. 13–19.
- [10] A. Alfieri, A. Bianco, P. Brandimarte, and C.-F. Chiasserini, "Maximizing system lifetime in wireless sensor networks," *European Journal of Operational Research*, vol. 181, no. 1, pp. 390–402, 2007.
- [11] G. Alirezaei, M. Reyer, and R. Mathar, "Optimum power allocation in sensor networks for passive radar applications," *Wireless Communications, IEEE Transactions on*, vol. 13, no. 6, pp. 3222–3231, 2014.
- [12] G. Alirezaei, O. Taghizadeh, and R. Mathar, "Optimum power allocation in sensor networks for active radar applications," *Wireless Communications, IEEE Transactions on*, to be published after November 2014.
- [13] I. Gradshteyn, I. Ryzhik, A. Jeffrey, and D. Zwillinger, *Table of Integrals, Series, and Products*, 7th ed. Academic Press, 2007.
- [14] A. W. Marshall, I. Olkin, and B. C. Arnold, *Inequalities: Theory of Majorization and Its Applications*, 2nd ed. New York: Springer, 2011.